JOURNAL OF GUIDANCE, CONTROL, AND DYNAMICS
Vol. 44, No. 3, March 2021

Engineering Notes

Feedback Control and Parameter Estimation for Lift Maximization of a Pitching Airfoil

Justin M. Lidard,* Debdipta Goswami,† and David Snyder‡
Princeton University, Princeton, New Jersey 08544
and
Girguis Sedky,§ Anya R. Jones,¶ and Derek A. Paley**
University of Maryland, College Park, Maryland 20742

https://doi.org/10.2514/1.G005441

Nomenclature

A	=	Jacobian matrix of linearized dynamics
AR	=	wing aspect ratio
C_D	=	drag coefficient
C_L	=	lift coefficient
c	=	mean aerodynamic chord
$\mathcal{F}$	=	equations of motion
f_0	=	steady-state flow stagnation function
$\mathcal{H}$	=	observation equation
k_1, k_2	=	control gains
k_1^*, k_2^*	=	optimal control gains
m_1, m_2	=	slopes of lift curve
Q	=	process noise covariance matrix
R	=	observation covariance matrix
T	=	time span of an orbit in phase space
U	=	wing towing speed
x	=	flow stagnation point
$\tilde{y}$	=	measured lift coefficient
z	=	state vector
α	=	angle of attack
α_{MAX}	=	maximum pitch angle
α_{STALL}	=	quasistatic stall angle
α_0	=	bias of post-stall linear regression
β_i	=	tuning parameter of the stagnation function, $i = 1, \ldots, 4$
γ	=	real part of eigenvalue
$\lambda_{1,2}$	=	eigenvalues of linearized system
$\sigma_{\tilde{y}}^2$	=	variance of measurement noise
$\sigma_{z_1}^2, \sigma_{z_2}^2$	=	variance of process noise
τ_1, τ_2	=	flow settling time constants
Ω	=	orbit in phase space
ω	=	imaginary part of eigenvalue

Presented as Paper 2020-1836 at the AIAA Scitech 2020 Forum, Orlando, FL, January 6–10, 2020; received 7 June 2020; revision received 18 October 2020; accepted for publication 28 November 2020; published online 7 January 2021.

*Graduate Research Assistant, Department of Mechanical and Aerospace Engineering. Student Member AIAA.
†Postdoctoral Research Associate, Department of Mechanical and Aerospace Engineering. Member AIAA.
‡Graduate Research Assistant, Department of Mechanical and Aerospace Engineering. Student Member AIAA.
§Ph.D. Candidate, Department of Aerospace Engineering. Student Member AIAA.
¶Associate Professor, Department of Aerospace Engineering. Associate Fellow AIAA.
**Willis H. Young Jr. Professor of Aerospace Engineering Education, Department of Aerospace Engineering and Institute for Systems Research. Associate Fellow AIAA.

I. Introduction

UNSTEADY aerodynamics is central to research at the interface of fluid dynamics and control theory for low-Reynolds-number aircraft such as micro air vehicles (MAVs). The regulation and control of unsteady behavior is crucial for maintaining the stability of an MAV, which necessitates accurate modeling of their flight surfaces. When an airfoil experiences a rapid pitching motion, unsteady flow features delay the onset of stall. A dynamically pitching airfoil will typically stall at a higher angle of attack than a static airfoil, and periodic pitching introduces hysteresis loops whose amplitudes are proportional to pitching frequency and airfoil geometry. Although unsteady or dynamic stall has catalyzed the development of model characterization in fluid dynamics, an optimal control approach has not yet emerged. Earlier work [1–3] has used linear control laws to maximize the steady-state lift, whereas this Note describes a method to maximize the time-averaged lift using nonlinear feedback control.

Prior work on stabilization techniques for MAVs and airfoils encountering unsteady flow uses linear control techniques to drive complex and often nonlinear dynamic systems to equilibrium points or a steady state. For example, Williams et al. [1] present a method for lift-coefficient stability for a wing in an unsteady flow environment. They use flow control to realize a proportional-integral feedback loop. Sedky et al. [2] demonstrated transverse gust rejection for a finite wing in an experimental towing tank. Several works also present nonlinear control techniques to achieve lift actuation. Oduyela and Slegers [4] introduce articulated wings to create additional roll stability for MAVs during gust encounters. Bhatia et al. [5] performed an extensive study on the stabilization of a flapping-wing MAV in the presence of discrete gust encounters. They characterize the behavior of the nonlinear system in the neighborhood of equilibrium points using linearization. Greenblatt et al. [3] demonstrate a significant reduction in lift hysteresis using a sinusoidal flow actuator with a low-order model by Goman and Khrabrov [6], which we adopt here.

The Goman–Khrabrov (GK) model is a low-order, nonlinear representation of the effect on lift of unsteady flow features based on a pair of coupled first-order ordinary differential equations. Figure 1 demonstrates the accuracy of the GK model in characterizing both static and dynamic pitching maneuvers for a wing, where dynamic pitching typically involves a periodic pitch rate. The lift hysteresis loops exhibited in Fig. 1 are typical of this type of pitching behavior [1,3,6–8]. Although current literature implements the GK model for purposes of active flow control and stabilization in unsteady flow, we design a destabilizing behavior for the purpose of maximizing average lift, first discussed in [9]. As [3] suggests, a time-varying control input, e.g., sinusoidal actuation, can reduce hysteresis effects and thereby decrease lift perturbations. While transient aerodynamic loads, such as gusts, can induce a large load normal to a lifting surface [10], a sufficiently strong structure can exploit hysteresis effects to create positive lift perturbations through the feedback-control framework presented here.

The technical approach described in this Note is to regulate the pitching rate of an airfoil using feedback control in order to visit the high-lift regions of the GK-model state space accessible only to unsteady pitch angles. Using experimental towing tank data, the dynamic stall properties of an airfoil are captured via a parameter fit. By designing state and, eventually, output feedback controls, we remove the explicit time dependence of an open-loop sinusoidal

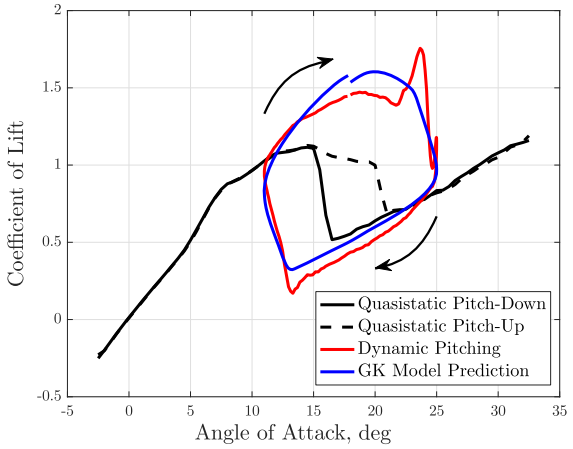

Fig. 1 Dynamic stall characteristics of an airfoil, comparing model behavior with experimental results. An airfoil's lift coefficient enters hysteresis loops near its stall angle [2].

input, which allows us to formally characterize the oscillations as a stable limit cycle of the dynamics. We analyze the closed-loop system using tools from bifurcation analysis and airfoil theory. Numerical results show that oscillating-pitch solutions boost the performance of the time-averaged lift by 40% over the optimal steady-pitch solution and by 65% over pre-stall conditions. Online estimation of model parameters using an extended Kalman filter (EKF) enables operation via a dynamic output-feedback control even when the GK time constants are unknown.

The contributions of this Note lie in the area of feedback-control design for lift augmentation. First, we present a nonlinear state-feedback control law to stabilize a limit cycle in the closed-loop GK model tuned to experimental data. The optimal unsteady behavior compares favorably with the best-case steady-state behavior. Secondly, the state-feedback control is extended to a dynamic output-feedback design using an EKF to assimilate noisy measurements of lift. The output-feedback control performance is comparable to the state-feedback case when the measurement noise variance is sufficiently small. The output-feedback control strategy includes online estimation of model parameters. The feedback control strategy presented here has the potential to enable aerospace vehicles with pitch-actuated airfoils and rotors to fly stably with higher time-averaged lift output while avoiding the adverse effects of stall.

The Note is organized as follows. Section II introduces the mathematical preliminaries of the GK model and the methodology for fitting the GK model to experimental data describing an airfoil's quasistatic lift profile. Section III presents the state-feedback design to stabilize a limit cycle that maximizes lift. Section IV describes the results and limitations of a closed-loop GK system with output feedback using sensor feedback of the lift coefficient, including optimization of feedback gains to maximize average lift. Section V describes a procedure for online estimation of the physical model parameters and the implementation of an output feedback strategy. Section VI summarizes the Note and ongoing work.

II. Goman–Khrabrov Model

A data-driven approach to modeling unsteady flow features can be effective at reducing the model dimensions [1–3,11]. The GK model provides an analytic characterization of the dynamics of flow separation on a wing based on static lift data. This Note adapts the GK model [6] for unsteady flow around an airfoil undergoing dynamic stall. The GK model is a two-state dynamic system consisting of an internal representation of the flow stagnation point $x \in [0, 1]$ measured along the chord line and the angle of attack α whose time evolution is defined by the following system of equations [6]:

$$\begin{aligned} \tau_1 \dot{x} + x &= f_0(\alpha - \tau_2 \dot{\alpha}) \\ \dot{\alpha} &= u \end{aligned} \tag{1}$$

where the time constants τ_1 and τ_2 are the flow settling times and u is the control input. The stagnation function f_0 describes the state of separation as deduced from an airfoil's alignment to pre- and post-stall lift curves. The time rate of change of the chordwise flow separation point for a dynamically pitching airfoil maps predictably as a function of angle of attack, but at higher or lower angles depending on the pitch rate.

Goman and Khrabrov present an analytic approximation for the coefficient of lift C_L, based on assumptions that the separated flow is modeled by linear cavitation theory [6]. In the original GK model, the coefficient of lift is nonlinear in x and α, i.e., [6]

$$C_L = \frac{\pi}{2}\left(1 + \sqrt{x}\right)^2 \sin\alpha \tag{2}$$

A generalized model of the coefficient of lift C_L at high angles of attack as a function of x and α is [1,3]

$$C_L = g_1(\alpha)x + g_2(\alpha)(1 - x) \tag{3}$$

For simplicity, $g_1(\alpha)$ and $g_2(\alpha)$ are assumed to be linear, i.e., $g_1(\alpha) = m_1\alpha$ and $g_2(\alpha) = m_2(\alpha - \alpha_0)$, although the resulting lift model (3) is still nonlinear. Figure 2 depicts the regressions $g_1(\alpha)$ and $g_2(\alpha)$ obtained from tow-tank lift curve data.

The GK model is applicable to a wide class of airfoils. The stagnation function f_0 may be determined experimentally in order to capture airfoil geometry and flow constants, including the Reynolds number. Although there is no constructive framework to derive f_0 from first principles, the boundedness of f_0 in the interval $[0, 1]$ can be used to produce an analytic approximation that captures its form and behavior. Because it is differentiable, we use an arctangent function with an argument shift, i.e.,

$$f_0(\alpha - \tau_2\dot{\alpha}) = \beta_1 - \beta_2 \arctan(\beta_3(\alpha - \tau_2\dot{\alpha} - \beta_4)) \tag{4}$$

where $(\beta_1, \beta_2, \beta_3, \beta_4)$ represent tuning parameters determined experimentally according to stall characteristics. Figure 3 compares the stagnation function (4) to experimental data [2] collected on an aspect ratio 4.9 wing at a Reynolds number of 40,000 in a water-filled tow tank. The wing chord length and towing speed are 0.115 m and 0.340 m/s, respectively, for a convective time c/U of 0.338 s.

The procedure for computing the parameters of the stagnation function (4) from the lift curve (3) is as follows. First, the static lift curve is generated by plotting the steady-state lift of an airfoil over a range of pitch angles. The lift curve is partitioned about the stall angle into two linear regions of distinct slopes. The slopes m_1 and m_2 are estimated via least squares as illustrated in Fig. 2. Once $g_1(\alpha)$ and $g_2(\alpha)$ are defined, Eq. (3) is inverted to solve for x. Finally, Eq. (4) is fit to the empirical data for x via nonlinear least squares using

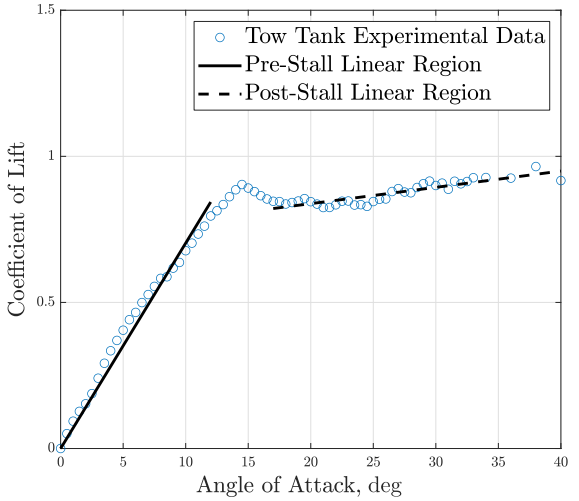

Fig. 2 Steady-state lift curve for a NACA 0012 finite wing obtained via an angle of attack sweep in a tow tank at $Re = 40{,}000$ [2].

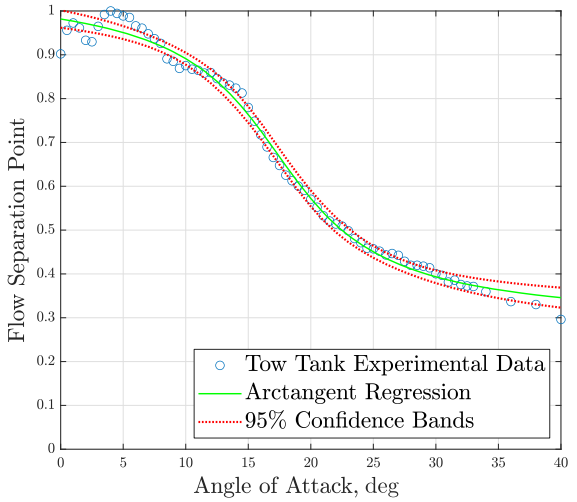

Fig. 3 Nonlinear parameter fit for the stagnation function f_0 using experimental data.

Table 1 Model parameters and values

Parameter	Name	Value	Unit	Source
β_1	Stagnation function vertical bias	0.6739	— —	Experimental data
β_2	Stagnation function amplitude	0.2464	— —	
β_3	Stagnation function stall rate	9.5090	rad^{-1}	
β_4	Stagnation function phase lag	0.3051	rad	
m_1	Pre-stall lift curve slope	3.9382	rad^{-1}	
m_2	Post-stall lift curve slope	0.3196	rad^{-1}	
α_0	Post-stall bias	0.7265	rad	
τ_1	Pitching sensitivity	0.296	— —	Estimated online
τ_2	Separation damping	2.959	— —	

MATLAB's *nlfit* (version R2019b). The static model parameter values solved in the regression are summarized in Table 1. The static parameters $(\beta_1, \beta_2, \beta_3, \beta_4)$ are obtained by fitting the experimental values. Also listed are nominal values of the dynamic time constants τ_1 and τ_2 (normalized by the convective time c/U) following the condition $\tau_2/\tau_1 \geq 10$ [6]; nominal values are independent of the other parameters and later approximated via online parameter estimation. The output equation parameters (m_1, m_2, α_0) are assigned via linear regression of two separate regions of the lift curve as shown in Fig. 2. Although the values in Table 1 were obtained using a NACA 0012 with particular flow conditions, the procedure presented in this note is general and can be used to capture airfoil–flow interactions for a wide class of geometries and flow conditions.

Although thin airfoil theory fails to provide a closed-form analytic model for drag on an airfoil [12], the following model captures the dramatic increase in drag introduced by high angles of attack. Let C_{D0} represent the parasitic and form drag. The coefficient of drag is [12]

$$C_D = C_{D0} + \frac{C_L^2}{\pi e AR} \tag{5}$$

Even if the exact induced drag characteristics of the wing used in testing are not known, the behavior of the drag coefficient is enough to characterize the drag produced at large angles of attack [12]. Small zero-lift drag is neglected to reflect the comparatively small effect of skin friction on the airfoil. A conservative span efficiency factor of $e = 0.7$ is used here to represent a nonelliptical planform.

The internal variable x can be derived from existing lift curve data for pre-stall and post-stall curves, where $x = 1$ represents fully attached flow and $x = 0$ denotes that the flow is fully separated. For example, a value of $x = 1$ returns a lift curve identical to an airfoil's standard pre-stall trend. x is not a direct measurement of flow stagnation, as no information related to freestream velocity, static pressure, or vorticity exists in this system. Rather, it can be thought of a representation of the flow attachment based on prior data-driven testing of the steady-state airfoil. Intermediate values between 0 and 1 reflect transient conditions. From Eq. (2), the nonlinear dependence of C_L on both α and x suggests that period oscillations in these parameters may produce lift that is higher, on average, than at constant α and x. This realization motivates a time-averaged, lift-maximizing control design using periodic pitching.

Next we express the equations of motion in state-space form. Let $z = (z_1, z_2) \triangleq (x, \alpha)$ and $y \triangleq C_L$. The modified GK model [6] is

$$\begin{aligned} \dot{z}_1 &= -\frac{1}{\tau_1} z_1 + \frac{1}{\tau_1}[\beta_1 - \beta_2 \arctan(\beta_3(z_2 - \tau_2 \dot{z}_2 - \beta_4))] \\ \dot{z}_2 &= u \\ y &= z_1 g_1(z_2) + (1 - z_1) g_2(z_2) \end{aligned} \tag{6}$$

In the sequel, we refer to the dynamics (6) as $\dot{z} = \mathcal{F}(z, u)$ and output $y = \mathcal{H}(z)$. With regard to the input u, it is possible to use a sinusoidal controller in the form $u(t) = A \sin(2\pi f t)$ to vary the pitch rate directly [3]. Alternatively, here we derive a state-feedback control of the form $u(z)$, because the closed-loop control more robustly incorporates sustained pitching while avoiding the aerodynamic penalties of stall. Then we implement this control law using measurements of the output y to estimate $\hat{z}$ to form an output feedback control law of the form $u(\hat{z})$. The dynamics in Eq. (6) are expanded to include the parameters (τ_1, τ_2) for output feedback, and the optimal control gains (k_1^*, k_2^*) to maximize the time-averaged lift are determined as a function of the estimated parameters $(\hat{\tau}_1, \hat{\tau}_2)$.

III. Feedback Control Design for the Goman–Khrabrov Model

The GK model provides a reduced-order modeling framework that we use to design a state-feedback control for maximizing the time-averaged lift. This section describes a nonlinear state-feedback control law that drives the airfoil dynamics to a limit cycle whose parameters can be optimized using average lift as a metric. In contrast to an open-loop sinusoidal input, a state-feedback control is robust to disturbances and model errors. Moreover, the closed-loop system is autonomous, which permits rigorous analysis in the phase plane.

A limit cycle is stabilized by destabilizing the static equilibrium point. Consider the linear state-feedback controller, $u = -k_1 z_1 - k_2 z_2$, which drives the system to a static equilibrium point. Using the GK lift coefficient given by Eq. (3), there is no steady pitch angle that achieves the same lift performance as periodic pitching, which also avoids stall. Alternatively, consider the nonlinear state-feedback law

$$u = k_1 z_1 - k_2 z_2^3 \tag{7}$$

where k_1 and k_2 are positive control gains. Note that setting $k_1 < 0$ emulates the linear control, using a cubic term for z_2 instead of a linear term. Figure 4a depicts the nullclines for angle of attack, i.e., $\dot{z}_2 = 0$, for several values of the ratio k_2/k_1 superimposed on the heat map of the lift coefficient over the state space. Also shown is the open-loop nullcline for the flow separation point, i.e., $\dot{z}_1|_{u=0} = 0$. The open-loop flow-separation nullcline (blue) represents the set of possible steady-state equilibrium points, which do not access the high lift regions (yellow). The intersection of the flow separation and angle-of-attack nullclines is an equilibrium point of the model such that $\dot{z} = 0$ for given values of k_1 and k_2. The maximum lift for a steady pitch angle is obtained from maximizing the output equation (3) over the set of all possible equilibrium points, i.e., the open-loop flow separation nullcline. Figure 4b shows the same nullclines superimposed over the lift-to-drag ratio with the maximum lift-to-drag ratio occurring at steady pitch. Figure 4 also plots the GK model nullclines, i.e., the contours where $\dot{z}_1$ and $\dot{z}_2$ are equal to zero.

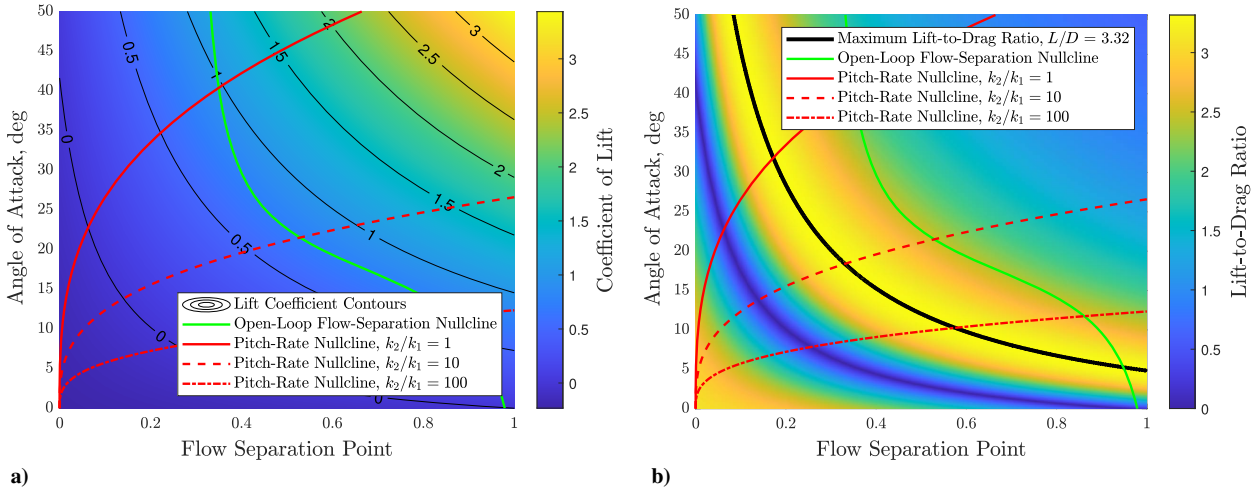

Fig. 4 a) Lift coefficient in the phase plane and b) lift-to-drag ratio as a function of the lift coefficient.

The closed-loop system (6) with the nonlinear control (7) stabilizes a limit cycle for certain values of the gains k_1 and k_2. To see this, observe that the equilibrium points of the GK model satisfy $\dot{z}_1 = 0$ and $\dot{z}_2 = 0$, which implies

$$\frac{k_2}{k_1} z_2^3 = f_0(z_2) \tag{8}$$

Let z_2^* represent a solution to the equilibrium condition (8). The Jacobian of the closed-loop system evaluated at z_2^* is

$$A \triangleq \left.\frac{\partial \mathcal{F}}{\partial z}\right|_{z_2 = z_2^*} = \begin{bmatrix} \frac{1}{\tau_1}\left(\frac{k_1 \tau_2 \beta_2 \beta_3}{1 + (\beta_3(z_2^* - \beta_4))^2} - 1\right) & -\frac{\beta_2 \beta_3}{\tau_1}\left(\frac{1 + 3k_2\tau_2 (z_2^*)^2)}{1 + (\beta_3(z_2^* - \beta_4))^2}\right) \\ k_1 & -3k_2 (z_2^*)^2 \end{bmatrix} \tag{9}$$

The eigenvalues of A are

$$\lambda_{1,2} = \frac{1}{2}\left(\mathrm{tr}\{A\} \pm \sqrt{(\mathrm{tr}\{A\})^2 - 4\,\mathrm{det}\{A\}}\right) \tag{10}$$

If the control gain k_1 is allowed to vary while the control gain k_2 is held fixed, then the real and imaginary parts of the eigenvalues (10) may be considered functions of a bifurcation parameter k_1, i.e.,

$$\lambda_{1,2}(k_1) = \gamma(k_1) \pm \omega(k_1) \tag{11}$$

Figure 5 illustrates how the eigenvalues of the closed-loop system cross the imaginary axis with nonzero velocity as the bifurcation parameter k_1 is quasistatically increased. This behavior is consistent with a supercritical Hopf bifurcation [13,14], which gives rise to a stable limit cycle that corresponds to the desired oscillating trajectory. Figure 6a shows the shape of the limit cycle in phase space. Note that

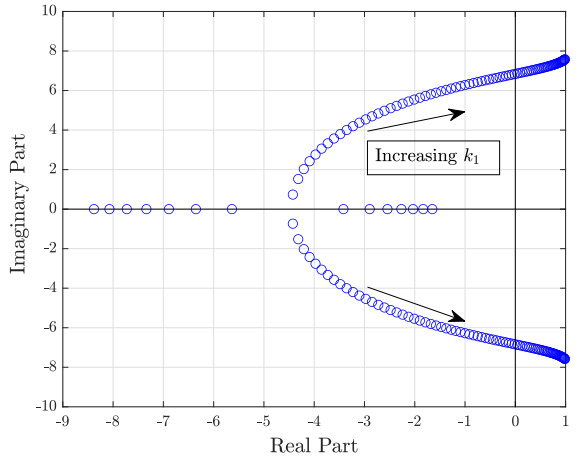

Fig. 5 Poles of the linearized, closed-loop system as a function of the control gain k_1.

the limit cycle (green) contains an unstable equilibrium point and is thus attracting for interior as well as exterior initial conditions.

Next we describe how to optimize the feedback control gains to maximize the time-averaged lift. Figure 6b depicts the average lift over all control gains k_1 and k_2 that stabilize a permissible limit cycle, i.e., a limit cycle that remains in the region of model validity. (Without loss of generality, assume an upper limit of $\alpha_{\mathrm{MAX}} = 50°$ for the angle of attack; the analysis can be performed for any such limit.) To determine the optimal gains, time series simulation data of (z_1, z_2) were computed for a 100×100 grid of gain values.

The time-averaged lift $\bar{C}_L$ is approximated here using the *trapz* function in MATLAB. The 10 s average (closed-orbit) lift obtained using the limit-cycle control is tabulated as shown in Fig. 6b. The optimal gain for the model parameters in Table 1 is $(k_1^*, k_2^*) = (9.70, 18.69)$, which produces a time-averaged lift coefficient of $\bar{C}_L = 1.46$. The steady-state maximum possible lift coefficient is $\bar{C}_L = 1.06$, evaluated at $z_2 = \alpha_{\mathrm{MAX}}$ (see Fig. 4). If the airfoil's stall angle is considered instead to be the maximum static-pitch angle, then steady-state maximum possible lift coefficient is $\bar{C}_L = 0.90$ evaluated at $z_2 = \alpha_{\mathrm{STALL}}$ as depicted in Fig. 2. Figure 7a shows the orbit with optimal limit cycle shape determined by the control gains. The intersection of the flow separation (green) and pitch (red) nullclines marks the initial state in the transition from static pitch equilibrium to dynamic pitching (black orbit). The limit cycle is highlighted in green. Figure 7b shows the time-averaged lift improvements versus the steady state upper bound. The nonlinear (unsteady) control performs approximately 40% better than linear (steady)

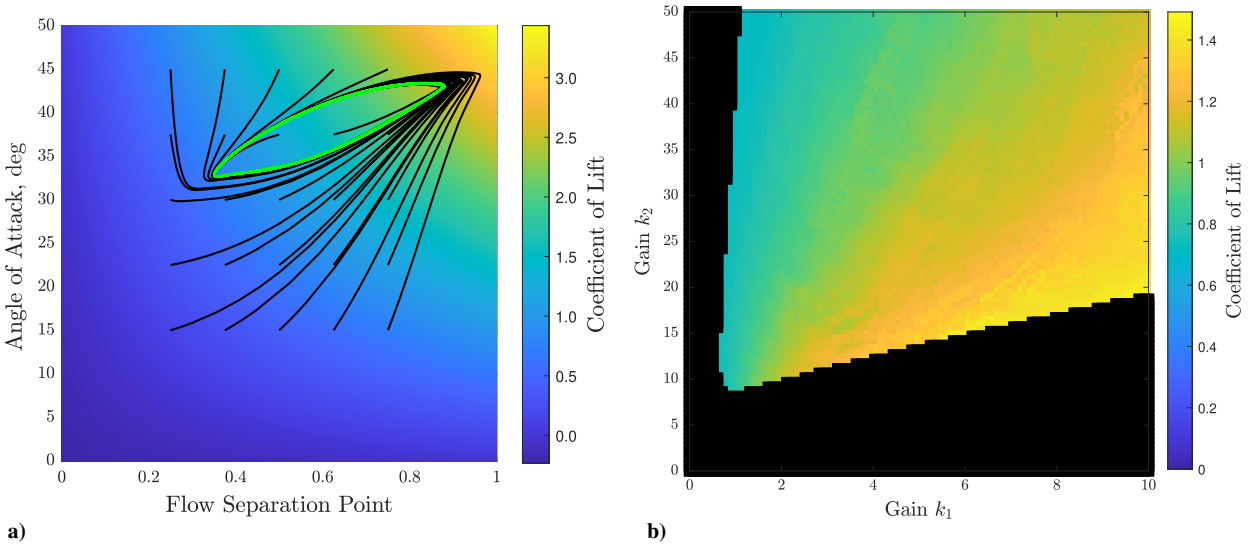

Fig. 6 a) Stable limit cycle for the closed-loop system in the phase plane and b) average lift performance of the closed-loop system for gain values that stabilize a limit cycle.

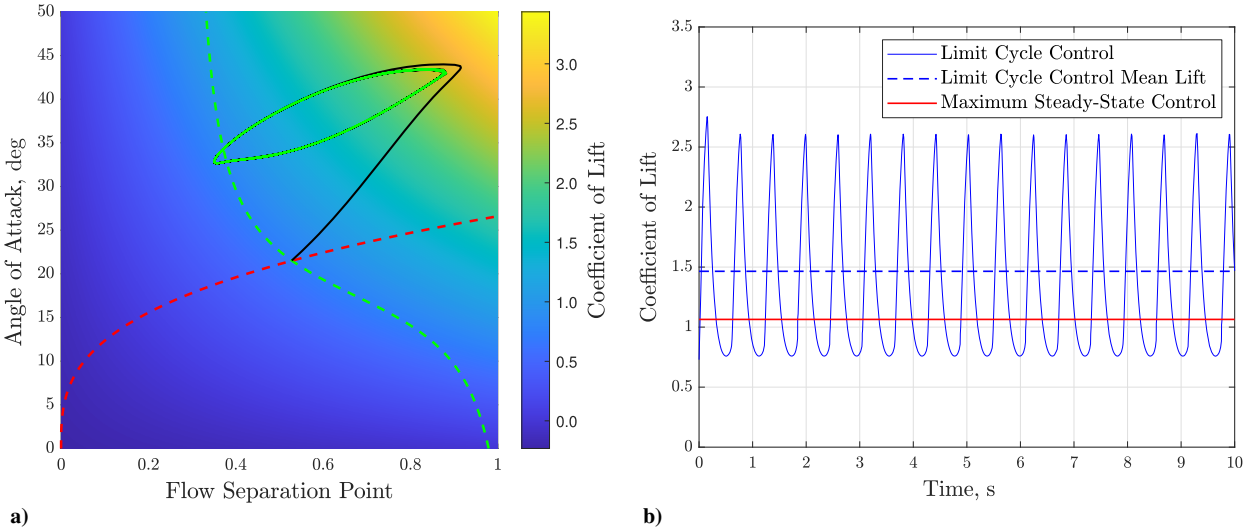

Fig. 7 a) The optimal limit-cycle control in phase space and b) lift coefficient output over time.

control when quasistatic stall is permitted and 65% when quasistatic stall is not permitted, using lift as a metric. However, the linear control performs better when using as metric the average ratio of lift to drag as shown in Fig. 4b. Therefore, the limit-cycle control framework presented here may be useful for commanding stable, high-lift heaving maneuvers.

IV. Output Feedback Control

The nonlinear feedback design above is a state-feedback control that requires the precise values of the state variables to be implemented. However, the flow-separation point z_1 is not measured directly. Here we design a filter to recursively estimate z_1 and z_2 from noisy measurements of the lift coefficient $y = C_L$ and angle of attack α. Then we implement an output-feedback controller by replacing the state variable in the nonlinear controller with the estimated values $\hat{\boldsymbol{z}} = (\hat{z}_1, \hat{z}_2)$.

Consider the state-space equations (6). Let $\boldsymbol{w}$ be zero-mean uncorrelated Gaussian process noise with covariance $Q = \text{diag}\{\sigma_{z_1}^2, \sigma_{z_2}^2\}$ and v be zero-mean uncorrelated Gaussian measurement noise with variance $R = \sigma_y^2$. The state and output equations have the general form

$$\begin{aligned} \dot{\boldsymbol{z}} &= \mathcal{F}(\boldsymbol{z}, u) + \boldsymbol{w} \\ \tilde{y} &= H(\boldsymbol{z}) + v \end{aligned} \tag{12}$$

where $\tilde{y}$ denotes the measured signal plus noise. The first equation describes the time evolution of the system states and the second allows them to be estimated from measurements.

We implement a discrete-time EKF by discretizing the dynamics and observation equations. Assume a uniformly distributed initial prior and nominal state estimate $\boldsymbol{z}_0$. The MATLAB *extendedKalmanFilter* class (version R2019B) was used to perform the prediction and update stages. The inputs to the *extendedKalmanFilter* class were the discrete-time measurement function $\boldsymbol{F}$, output function $\mathcal{H}$, covariance matrices Q and R, time step 10 ms, and initial estimate $\hat{\boldsymbol{z}}_0$. Because the continuous time state transition equation $\mathcal{F}$ is nonlinear, the discretized state transition $\boldsymbol{F}$ can be approximated by taking the last value in the time series returned by MATLAB's *ode45* over a small time step. At each time t, the state estimate $\hat{\boldsymbol{z}} = (\hat{x}, \hat{\alpha})$ is used to compute the control input $u(\hat{x}, \hat{\alpha})$.

An important requirement of the output-feedback control is the preservation of the limit-cyclic behavior, which allows lift augmentation to continue indefinitely. Figure 8 shows that the output-feedback control with an EKF preserves limit-cyclic behavior, thereby preserving the high average lift. Adherence to the optimal limit cycle in each iteration is a function of the measurement noise covariance, as depicted in Fig. 8. Figure 9 compares the lift coefficient time series obtained from the trajectories depicted in Fig. 8. These results show that large-amplitude oscillations are necessary to maintain high pitching rate and

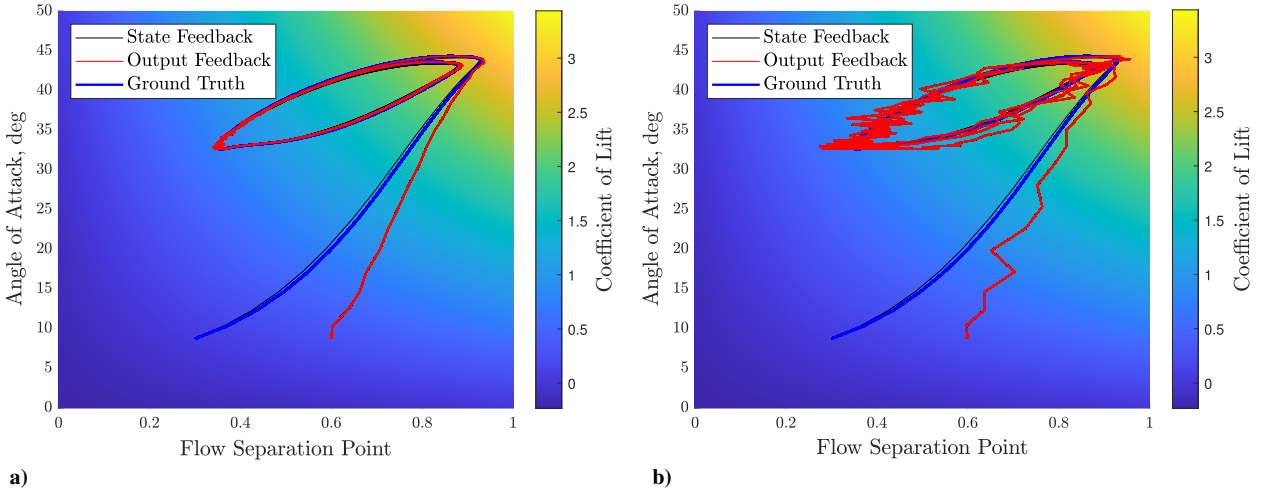

Fig. 8 Limit cyclic behavior is preserved with output feedback, although adherence to the state feedback trajectory is a function of measurement noise σ_y: a) $\sigma_y = 0.01$; b) $\sigma_y = 0.1$.

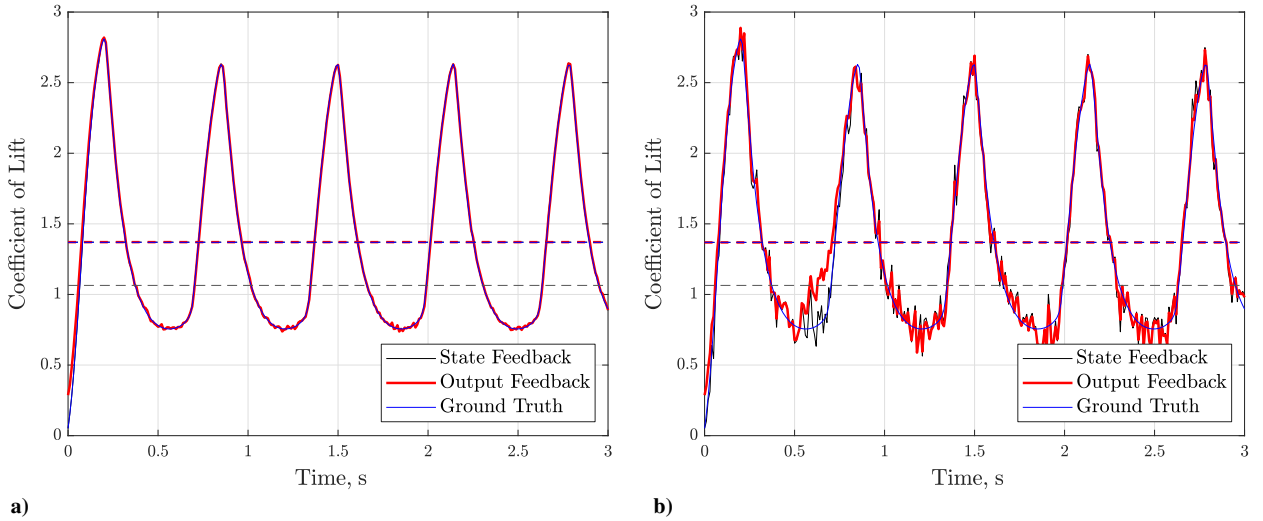

Fig. 9 Coefficient of lift versus time for the trajectories in Fig. 8 and the optimal steady-state coefficient of lift (gray).

lift output, avoiding stall. As a direct consequence of the Hopf bifurcation (Sec. III), the pitching amplitude about equilibrium is initially small and symmetric with little change to the average lift. The pitching amplitude increases with the bifurcation parameter k_1, and the nonlinearities of the GK model permit access to high-lift regions of the state space. The optimal lift for given parameters τ_1 and τ_2 can be calculated by sweeping gain values k_1 and k_2. Furthermore, the next section describes how the optimal gains k_1^* and k_2^* can be controlled adaptively based on the online estimates of τ_1 and τ_2.

V. Online Parameter Estimation

In the original GK model (1), the parameters τ_1 and τ_2 are time constants that represent the settling properties of the flow surrounding the airfoil [6]. The parameter τ_1 determines the rate of convergence for the flow separation point to return to the steady state. The parameter τ_2 determines the sensitivity of stall to the pitch rate; higher τ_2 corresponds to more extreme fluctuations in the flow separation during rapid pitching. A table of optimal gains produced by sweeping over a grid of (τ_1, τ_2) returns the gains corresponding to the highest time-averaged lift control for each flow condition. Let (k_1^*, k_2^*) represent the optimal control gains for the time constants τ_1 and τ_2. This section describes methods to estimate τ_1 and τ_2 online.

As discussed in [15], model parameters can be estimated adaptively and simultaneously with the states by augmenting the state space to include the parameters. Specifically, we augment the model dynamics (6) by including $\dot{z}_3 = 0$ and $\dot{z}_4 = 0$, where the state vector becomes $\boldsymbol{z} = (x, \alpha, \tau_1, \tau_2)$. Hence, in the augmented discrete state transition equation, the process noise covariance becomes $Q = \text{diag}\{\sigma_{z_1}^2, \sigma_{z_2}^2, \sigma_{\tau_1}^2, \sigma_{\tau_2}^2\}$, whereas the measurement covariance R is unchanged. Note that this augmentation is simply an explicit representation of the assumed steady-state nature of the model parameters, which are constant. The inclusion of the process noise $\boldsymbol{w}$ describes the online variation of the parameters over time. The initial probability density function over the state space has a local maximum at the nominal values, τ_{10} and τ_{20}. Recursive expectation maximization produces $\hat{\tau}_1$ and $\hat{\tau}_2$ that minimize the error in the state estimate via the GK dynamics (1).

As discussed in Sec. III, the shape of the limit cycle in phase space is influenced by the gains of the control law in Eq. (7). Once the supercritical Hopf bifurcation is achieved, a larger magnitude of $\gamma(k_1)$ [see Eq. (11)] causes a larger amplitude cycle in phase space. For a given set of model parameters (τ_1, τ_2), a set of optimal gains (k_1^*, k_2^*) produces the highest time-averaged lift without exceeding $z_2 = \alpha_{\text{MAX}}$. Note that the model parameters we wish to estimate are not observable directly via the output equation (6) because y is not a function of τ_1 or τ_2. The zero dynamics for τ_1 and τ_2 means that the output y is only affected by these parameters via the flow separation. Therefore, estimation of τ_1 and τ_2 must be performed simultaneously with the estimation of the other states, as described next.

Nominal values representing ground truth initial parameters and states are generated first. Initial estimates are declared as the truth values plus additive noise. For a time range spaced by the time step τ,

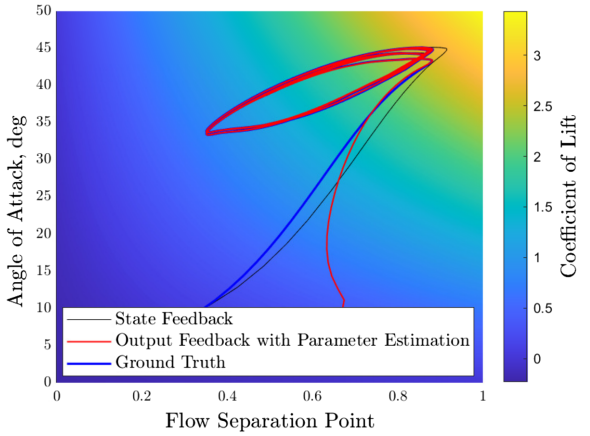

Fig. 10 Phase space representation of airfoil dynamic pitching with online estimation of the parameters τ_1 and τ_2 and adaptive control gains k_1 and k_2.

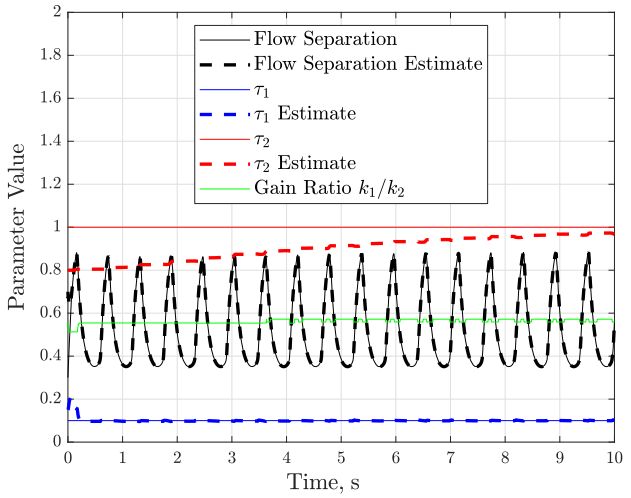

Fig. 11 Ground-truth and estimated signals for the state z_1 and parameters τ_1 and τ_2. The gain ratio converges to the optimal value as the estimates for τ_1 and τ_2 converge.

the plant dynamics in Eq. (1) are simulated using a fourth-order approximation, with the control input in Sec. IV. The lift measurement $\tilde{C}_L$ is generated using the truth values of the states z_1 and z_2 with noise σ_y and passed to the EKF to produce a state estimate $\hat{z} = (\hat{x}, \hat{\alpha}, \hat{\tau}_1, \hat{\tau}_2)$. The control gains are continually updated to the optimal value for given parameter estimates. Estimates are produced recursively as the system dynamics evolve until the end of simulation. Figure 10 shows the limit cycle expanding toward the high-lift region of state space as the model parameter estimates become better and the control gains optimal.

The time interval 10 ms of the EKF is small relative to the period of the limit cycle. Additionally, a limit cycle in the plane always contains a local equilibrium point [13,14]. Because any orbit stays within a finite neighborhood of the equilibrium point, the EKF is an appropriate estimation framework for the GK model assuming Gaussian process noise. Figure 11 shows that the EKF permits accurate reconstruction of the parameter and lift coefficient ground-truth values, with the control gains also becoming optimal (here expressed as a ratio k_1/k_2) as a function of the estimated parameters $\hat{\tau}_1$ and $\hat{\tau}_2$. Figure 12 plots the coefficient of lift and angle of attack generated over time for the orbit shown in Fig. 10 and provides a comparison to the state feedback and output feedback strategies discussed in Secs. III and IV via the maximum steady-pitch ($\alpha = \alpha_{\mathrm{MAX}}$) values shown in gray. Note that estimation of τ_1 and τ_2 causes the period of the output feedback limit-cycle control to more closely match that of the state feedback control. Convergence to within a small steady-state error <0.005 occurs in less than 0.33 s (0.97 when normalized by the convective time c/U) and corresponds to two full orbits of the limit cycle.

Because the values of τ_1 and τ_2 are not known initially, it is not feasible to apply the optimal control gains until the EKF converges. Consequently, the airfoil will not reach the best possible C_L during the transient response. The loss of lift due to uncertainty in τ_1 and τ_2 for a particular orbit Ω is calculated by taking the time-averaged difference in lift output between Ω and the orbit achieved via the same initial conditions with known τ_1 and τ_2.

The lift deficit for orbits corresponding to the same initial conditions presented in Fig. 10 is shown in Fig. 13, with black squares representing orbits that fail to produce a valid limit cycle. The marginal increase in lift around the center of the figure reflects the many local extrema in the plane of possible gains, as the gradient is plausibly small in magnitude over a large region (see Fig. 6). However, Fig. 13 also suggests that it is necessary to estimate τ_1 and τ_2 in order to avoid invalid limit cycles or orbits.

VI. Conclusions

This Note proposes state- and output-feedback controls for a pitching airfoil in an unsteady flow using the Goman–Khabrov model. Because the coefficient of lift undergoes hysteresis at or near stall, the proposed feedback control generates by design a stable limit cycle. The resulting periodic pitching trajectory yields a 40% increase in time-averaged lift compared with the maximum steady pitch angle. However, a steady pitch angle maximizes the lift-to-drag

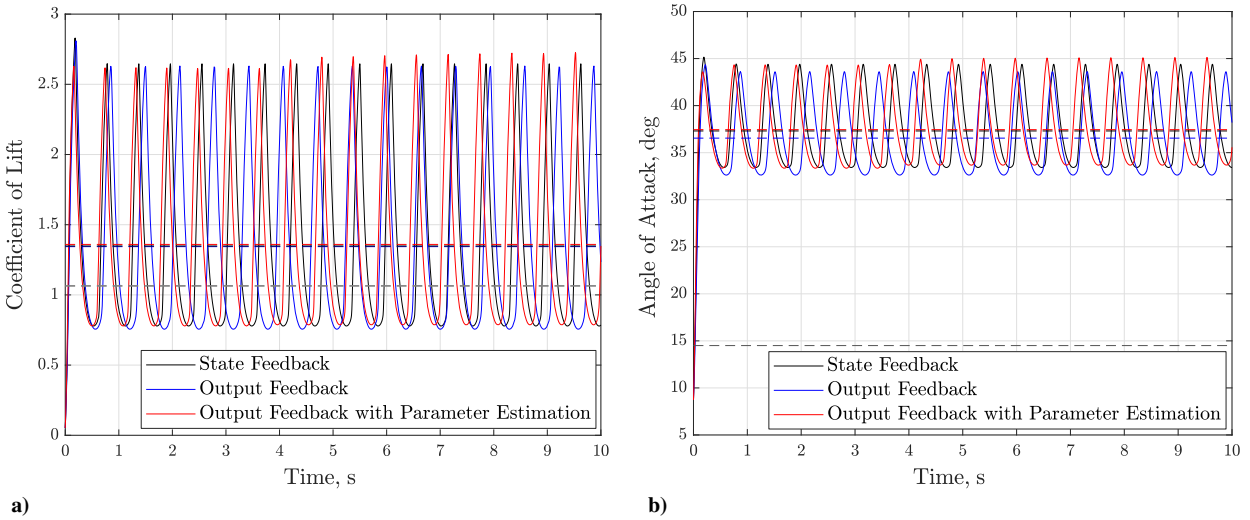

a) b)

Fig. 12 a) Coefficient of lift versus time and b) angle of attack versus time for various feedback strategies.

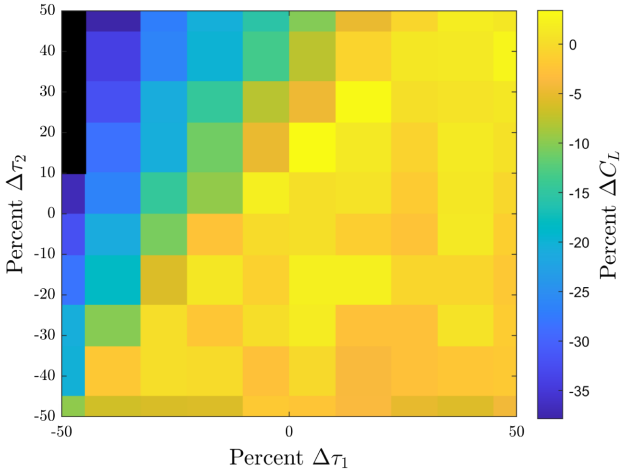

Fig. 13 Percent change in average lift due to percent error in the model parameters τ_1 and τ_2.

ratio. The EKF is used to implement the output feedback strategy, including online estimation of the model parameters. The estimated parameter values determine the optimal control gains using a lookup table.

Acknowledgments

This work was partially supported by Air Force Office of Scientific Research Grant Nos. FA9550-18-1-0137 and FA9550-16-1-0508. We also acknowledge preliminary discussions with Frank Lagor related to this work.

References

[1] Williams, D., Kerstens, W., Buntain, S., Quach, V., Prieffer, J., King, R., Tadmor, G., and Colonius, T., "Closed-Loop Control of a Wing in an Unsteady Flow," *48th AIAA Aerospace Sciences Meeting Including the New Horizons Forum and Aerospace Exposition*, AIAA Paper 2010-0358, 2010, pp. 1–8. https://doi.org/10.2514/6.2010-358

[2] Sedky, G., Jones, A. R., and Lagor, F., "Lift Regulation During Transverse Gust Encounters Using a Modified Goman Khrabrov Model," *AIAA Journal*, Vol. 58, No. 9, 2020, pp. 3788–3798. https://doi.org/10.2514/1.J059127

[3] Greenblatt, D., Muller-Vahl, H., Srimanta, S., Williams, D., and Reissner, F., "Feed-Forward Control for Goman-Khrabrov (G-K) Model on Pitching Airfoils with Flow Control," *8th AIAA Flow Control Conference*, AIAA Paper 2016-4240, 2016, pp. 1–11. https://doi.org/10.2514/6.2016-4240

[4] Oduyela, A., and Slegers, N., "Gust Mitigation of Micro Air Vehicles Using Passive Articulated Wings," *Scientific World Journal*, Vol. 2014, Jan. 2014, pp. 1–10. https://doi.org/10.1155/2014/598523

[5] Bhatia, M., Patil, M., Woolsey, C., Stanford, B., and Beran, P., "Stabilization of Flapping-Wing Micro-Air Vehicles in Gust Environments," *Journal of Guidance, Control, and Dynamics*, Vol. 37, No. 2, 2014, pp. 592–607. https://doi.org/10.2514/1.59875

[6] Goman, M., and Khrabrov, A., "State-Space Representation of Aerodynamic Characteristics of an Aircraft at High Angles of Attack," *Journal of Aircraft*, Vol. 31, No. 5, 1994, pp. 1109–1115. https://doi.org/10.2514/3.46618

[7] Williams, D. R., Rießner, F., Greenblatt, D., Müller-Vahl, H., and Strangfeld, C., "Modeling Lift Hysteresis on Pitching Airfoils with a Modified Goman–Khrabrov Model," *AIAA Journal*, Vol. 55, No. 2, 2017, pp. 403–409. https://doi.org/10.2514/1.J054937

[8] Brunton, S. L., Rowley, C. W., and Williams, D. L., "Reduced-Order Unsteady Aerodynamic Models at Low Reynolds Numbers," *Journal of Fluid Mechanics*, Vol. 724, June 2013, pp. 203–233. https://doi.org/10.1017/jfm.2013.163.

[9] Lidard, J., Goswami, D., Snyder, D., Sedky, G., Jones, A. R., and Paley, D. A., "Output Feedback Control for Lift Maximization of a Pitching Airfoil," *AIAA SciTech Forum*, AIAA Paper 2020-1836, 2020. https://doi.org/10.2514/6.2020-1836

[10] Williams, D., and King, R., "Alleviating Unsteady Aerodynamic Loads with Closed-Loop Flow Control," *AIAA Journal*, Vol. 56, No. 6, 2018, pp. 2194–2207. https://doi.org/10.2514/1.J056817

[11] Gomez, D. F., Lagor, F. D., Kirk, P. B., Lind, A. H., Jones, A. R., and Paley, D. A., "Data-Driven Estimation of the Unsteady Flowfield Near an Actuated Airfoil with Embedded Pressure Sensors," *Journal of Guidance, Control, and Dynamics*, Vol. 42, No. 10, 2019, pp. 2279–2287. https://doi.org/10.2514/1.G004339

[12] Anderson, J., *Fundamentals of Aerodynamics*, 5th ed., McGraw–Hill, New York, 2007, pp. 427–464, Chap. 5. https://doi.org/10.1017/S000192400000676X

[13] Marsden, J. E., and McCracken, M., *The Hopf Bifurcation and its Applications*, 19th ed., Springer-Verlag, New York, 1976, pp. 1–84, Chaps. 1–4. https://doi.org/10.1016/0022-247X(79)90207-5

[14] Strogatz, S. H., *Nonlinear Dynamics and Chaos: With Applications to Physics, Biology, Chemistry, and Engineering*, 1st ed., Perseus, New York, 1995. https://doi.org/10.1063/1.2807947

[15] Maasoumy, M., Moridian, B., Razmara, M., Shahbakhti, M., and Sangiovanni-Vincentelli, A., "Online Simultaneous State Estimation and Parameter Adaptation for Building Predictive Control," *2013 ASME Dynamic Systems and Control Conference*, American Soc. of Mechanical Engineers, Fairfield, NJ, 2014, pp. 1–10, https://manufacturingscience.asmedigitalcollection.asme.org/DSCC/proceedings-abstract/DSCC2013/56130/V002T23A006/228594. https://doi.org/10.1115/DSCC2013-4064